J. Fluid Mech. (2000), *vol.* 424, *pp.* 217–241. Printed in the United Kingdom

Numerical simulation of turbulent flow in a pipe oscillating around its axis

By MAURIZIO QUADRIO AND STEFANO SIBILLA

Dipartimento di Ingegneria Aerospaziale del Politecnico di Milano,
Campus Bovisa – via La Masa 34 – 20156 Milano, Italy

(Received 29 September 1999 and in revised form 13 June 2000)

The turbulent flow in a cylindrical pipe oscillating around its longitudinal axis is studied via direct numerical solution of the Navier–Stokes equations, and compared to the reference turbulent flow in a fixed pipe and in a pipe with steady rotation. The maximum amount of drag reduction achievable with appropriate oscillations of the pipe wall is found to be of the order of 40%, hence comparable to that of similar flows in planar geometry. The transverse shear layer due to the oscillations induces substantial modifications to the turbulence statistics in the near-wall region, indicating a strong effect on the vortical structures. These modifications are illustrated, together with the implications for the drag-reducing mechanism. A conceptual model of the interaction between the moving wall and a streamwise vortex is discussed.

1. Introduction

Friction drag in turbulent wall flows is several times higher than in laminar flows. This is one of the main motivations for studies on turbulence management. Many of them are aimed at reducing the friction drag while allowing the flow to remain turbulent, both by using an external energy source (i.e. *active* techniques) or by relying on effects, like the modification of the shape of the wall (*passive* techniques), which do not require any external energy to be put into the system. The industrial importance and potential of such studies is enormous.

A recently discovered method for achieving a sustained turbulent drag reduction in boundary layers and channel flows is a cyclic movement of the wall, of appropriate amplitude and frequency, in the spanwise direction. This clearly represents an active technique, since energy is needed for the motion of the wall, but it offers the remarkable advantage of being rather simple from a conceptual point of view, since no feedback is required in the control law. The use of this technique was first suggested by Jung, Mangiavacchi & Akhavan (1992), who have been able to show, via a direct numerical simulation (DNS), that reductions of friction drag of the order of 40% are possible, by carefully selecting the parameters of the oscillation. These results have been further confirmed by the subsequent DNS of Baron & Quadrio (1996). They contributed the additional information that not only is a significant drag reduction possible, but also the overall energetic balance, computed by taking into account the power spent for the movement of the wall, can be positive. On the experimental side, studies by Laadhari, Skandaji & Morel (1994), Skandaji (1997), Choi *et al.* (1997), and Trujillo, Bogard & Ball (1997), have confirmed and extended the DNS results. More recently, Dhanak & Si (1999) have also proposed a conceptual model for explaining the effect of the lateral oscillations on the turbulent friction.

To date, most of the studies, both experimental and numerical, conducted on the subject of spanwise wall oscillations, have focused on plane channel flows and boundary layers, owing to the combined generality and simplicity of such geometries. Only recently, has an experimental study by Choi & Graham (1998) addressed the case of turbulent flow in a *cylindrical pipe* subject to oscillations around its longitudinal axis. According to the authors, this setup holds 'great promise for industrial applications, for example, in the transport of oil, gas, water and foodstuffs through pipes'. We are unaware of similar research conducted numerically via DNS; however, a numerical simulation of the turbulent flow in a pipe has been provided by Eggels *et al.* (1994), to whom we will refer to as EUW in the following. Orlandi & Fatica (1997, hereinafter referred to as OF) performed similar computations, and, in addition, were able to investigate the effect of a steady rotation of the pipe about its longitudinal axis, exploring a wide range of rotation numbers, and finding that in the presence of steady rotation the flow experiences a decrease of the friction factor.

The case with alternating rotation, the subject of the present study, is different from the case with steady rotation. As will be seen in the following, not only can the amount of drag reduction be significantly higher, but, more important, the overall structure of the flow looks completely different in the wall region, and hence the modification induced by the rotation on the turbulent structures also shows significant differences.

Besides the practical interest for drag reduction, the oscillating flow studied in the present work is interesting *per se*, since it represents a flow where the wall vorticity induced by the movement of the wall is aligned with the streamwise vortices. Their role and importance in the turbulence-production cycle is recognized by many authors, see for example Robinson (1991). This is the case also for the steady rotating pipe investigated by OF, but in their study the induced mean vorticity greatly influences the flow, while here the time-averaged value of the vorticity related to the rotation of the wall is zero. It can be therefore interesting to look at the direct effects of a zero-mean streamwise vorticity distribution imposed on a turbulent pipe flow.

The structure of the paper is as follows. The physical problem, the numerical techniques and the computational parameters are described in § 2. In § 3 results are presented for the preliminary parametric study focused on drag reduction, while turbulence statistics obtained with finer mesh computations are illustrated in § 4. A tentative explanation of the interaction between the moving wall and near-wall turbulence structures is discussed in § 5.

2. Physical problem and numerical techniques

Three turbulent flows have been simulated: one in a fixed pipe, one in a steadily rotating pipe and the last in the oscillating pipe.

The equations of motion have been made non-dimensional with the centreline streamwise velocity U_P of the laminar Poiseuille flow which possesses the same bulk mean velocity U_b as the actual flow, and by the radius R of the pipe. The Reynolds number has consequently been defined as $Re = U_P R/\nu$, and it has been set to $Re = 4900$ for the reference flow. In the steady rotating pipe flow, the rotation number is $N = 2\Omega R/U_P$, where Ω is the angular velocity of the pipe; in the oscillating pipe flow, N is defined as $N = 2v_{\theta 0}/U_P$, where $v_{\theta 0}$ is the maximum amplitude of the oscillation of the pipe wall. The azimuthal component of the wall velocity is therefore given by $v_\theta = v_{\theta 0} \sin\left(2\pi t/T_w\right)$; here T_w is the period of the sinusoidal oscillation.

Computations have been carried out by keeping the bulk mean velocity fixed (which

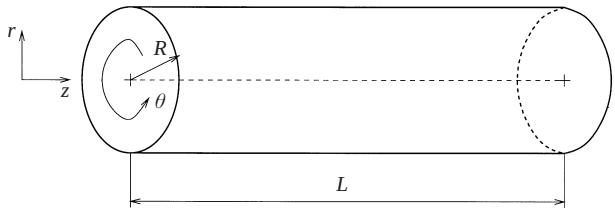

FIGURE 1. Sketch of the computational domain.

is 0.5 with the present non-dimensionalization), and hence the mean pressure gradient varies with time.

A parametric study has been performed, to determine the best parameters in terms of drag reduction. Three oscillation periods have been tested: $T_w^+ = 50$, 100 and 150. The plus superscript indicates (here and in the following) quantities in wall units, i.e. made non-dimensional with the kinematic viscosity and the friction velocity $u_\tau = \sqrt{\tau_w/\rho}$, where τ_w is the computed wall friction and ρ is the fluid density. For each period five rotation numbers have been used, from $N = 0$ to $N = 1$ in steps of 0.2.

The computer code used for the present research was developed by Verzicco & Orlandi (1996), and a detailed description is given in their paper, where two-dimensional, axisymmetric and three-dimensional flows are computed for the purpose of validation. The code is a solver for the Navier–Stokes equations written in primitive variables and in cylindrical coordinates. Figure 1 is a sketch of the computational domain, where z indicates the axial direction, θ is the azimuthal angle and r the radial coordinate. The variables actually used in the code are $q_\theta = rv_\theta$, $q_r = rv_r$ and $q_z = v_z$, since this choice reduces the problems associated with the singularity at $r = 0$ and allows better accuracy to be achieved in the axis region. The code is based on second-order finite-difference schemes for the spatial discretization of viscous and advective terms, and uses a fractional step method, based on the third-order low-storage Runge–Kutta method, for advancing the solution in time. Given that viscous terms are treated implicitly by the Crank–Nicholson scheme, the overall accuracy of the code is second order both in time and space. The code has been used for the simulation of the turbulent flow in a steady rotating pipe by OF. They employed a fixed reference frame, taking into account the steady rotation of the pipe via the presence of the Coriolis body force in the equations of motion.

In the present work, the code has been modified in order to account for the particular boundary conditions. Periodic conditions have been imposed in the longitudinal direction (the relevant effect of the domain length L/R on the results will be discussed in the following). In order to cope with the alternating movement of the cylindrical wall, we have decided to use an inertial laboratory reference frame, instead of translating the movement of the wall into a time-dependent body force. In this way the sinusoidal oscillation of the wall requires the application of the appropriate instantaneous velocity value as the boundary condition for the azimuthal component of the velocity at the wall.

The DNS of turbulent flows in pipes oscillating sinusoidally around the longitudinal axis is computationally expensive. There are two main factors affecting its cost. First, the time integration interval must be larger than that required for the simulation of the flow in a steady rotating pipe, due to the time required for the alternating oscillations to be felt from the wall through the whole pipe and to give rise to a statistically steady state. Second, the longitudinal extent of the computational domain

must be larger, in order to account for the elongation of the near-wall turbulent structures induced by the oscillation. We have used a pipe length of $L = 20R$, which has been proved to be the minimum for the assumption of periodicity in the axial direction to be valid. For the fixed pipe flow, a length of $L = 10R$ has been used by EUW, even though it does not allow all correlations to decrease to zero. In their study OF, after checking both $L = 15R$ and $L = 20R$, decided to use $L = 15R$ for the simulations of the rotating case. In the present case, $L = 20R$ is necessary, given the intense drag reduction and the consequent elongation of the structures in the axial direction. Examination *a posteriori* of the autocorrelation functions computed at some distances from the wall (see e.g. figure 12*c*) confirms the adequacy of this choice.

The results presented here have been computed using two mesh sizes. The coarser mesh has $97 \times 39 \times 97$ points, in the azimuthal, radial and longitudinal directions respectively, and is used in the preliminary study to determine the parameters of the oscillations leading to the best performance in terms of reduction of turbulent skin friction. The finer mesh has $129 \times 97 \times 257$ grid points; the corresponding resolutions are $\lambda^+ = (r\Delta\theta)^+ \leqslant 8.28$, $\Delta r^+ = 0.57$–3, and $\Delta z^+ = 13.3$. This mesh is used to compute the turbulence statistics described in § 4. The distribution of the mesh points in the radial direction follows a hyperbolic tangent, in order to enhance resolution in the wall region, where the turbulent length scales are smaller, while keeping reasonably low the number of grid points in the radial direction. The stretching is however kept very small, with the aim of avoiding the introduction of numerical inaccuracies. As will be illustrated later, *a posteriori* examination of power spectral density functions confirms that the spatial resolution of the most resolved simulation is adequate to represent the relevant turbulent scales in the flow. These resolutions are comparable to those used by Kim, Moin & Moser (1987) in their well-known work on plane channel flows, and by many other investigators in different DNS of similar flows at equivalent Reynolds numbers. One possible exception is Δr^+, which is in the range of the best-resolved finite-difference computations (e.g. those by OF), but might be smaller near the wall when different discretizations are used.

First a simulation for the steady pipe flow has been conducted. After reaching the statistically steady state, a single flow field has been chosen as the starting point for the other simulations with the oscillating pipe. These computations have been carried out for 600 non-dimensional time units (i.e. $600\,tU_P/R$), but the calculation of the mean friction was started after 200 time units, to let the initial transient completely disappear. Approximately 50 000 time steps are needed for the integration of the most demanding computational case. Nineteen and twenty-three flow fields have been stored for further analysis in the fixed and steadily rotating case respectively. For the oscillating pipe, to study the dependence of the statistics on the phase of the oscillation cycle, nineteen cycles (after the initial transient stage) have been analysed, by storing eight flow fields for each cycle, amounting to a total of 152 flow fields.

3. Parametric study of the drag-reduction effect

Several computations on a relatively coarse mesh have been performed to assess the turbulent drag-reduction properties of the oscillating pipe, and to compare its performance with that in the plane geometry (boundary layer or channel flow). The results of this parametric study are shown in figure 2, where the percentage drag reductions are reported vs. the maximum wall velocity. A rotation number of $N = 1$ corresponds to $v_{\theta 0}^+ \simeq 14$, made non-dimensional in wall units by using the friction velocity computed for $N = 0$. It has been verified that these results (in terms of

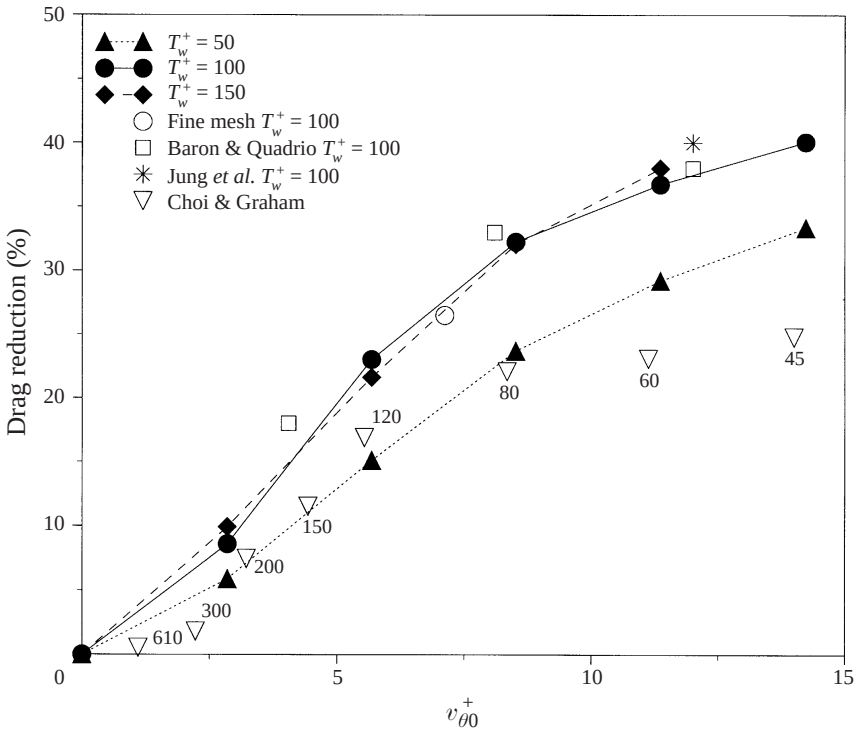

FIGURE 2. Reduction in friction drag for turbulent flow in the oscillating pipe, as a function of the non-dimensional wall velocity $v_{\theta 0}^+$, for different periods of oscillation. Comparison with data measured for plane channel flows at $T_w^+ = 100$ and with experiments for pipe flow at $Re = 23\,300$ (labelled with corresponding T_w^+). The open circle shows the result from the fine-mesh computation, at $N = 0.5$ and $T_w^+ = 100$.

friction reduction) are not affected by the spatial resolution. The time history of the friction does indeed depend on the resolution, but it has been found that its mean value does not. The data point, shown in figure 2 with an open circle and corresponding to $N = 0.5$ and $T_w^+ = 100$, has been computed with the fine mesh, and supports the claim of independence of the results from the mesh size, as far as the percentage drag reduction is concerned. Indeed, it falls on the line interpolating the coarse mesh data obtained for the same oscillation period.

It can be seen that the oscillation of the pipe can lead to a friction decrease as high as 40% with respect to the non-oscillating turbulent pipe, when the rotation number approaches unity. The range of $N > 1$ has not been investigated, but the curves seem to have a plateau at high N. These results are almost coincident with similar data obtained in the plane geometry; figure 2 reports measurements obtained via numerical simulations, for $T_w{}^+ = 100$, in channel flows at similar Reynolds number, by Jung *et al.* (1992) and Baron & Quadrio (1996).

Experimental data in the cylindrical geometry are available only from Choi & Graham (1998), but they are collected at the higher Reynolds numbers of 23 300 and 36 300 (based on pipe diameter). The reported maximum value of drag reduction is 25%. The experimental setup used by Choi & Graham (1998) allowed them to move the pipe wall while keeping the lateral excursion fixed, so that an increase of the wall velocity required an increase in the frequency of the oscillation. Consequently, Choi

& Graham's data plotted in figure 2 are measured at different values of the oscillation period (they are labelled in the figure with the actual value of T_w^+). While low Reynolds number effects cannot be excluded, it is possible that the difference in maximum drag reduction between the present work and the experimental measurements by Choi & Graham (1998) is due to their non-optimal value of the oscillation period for the highest wall speeds.

Following the analysis already developed by Baron & Quadrio (1996) for the plane channel flow with oscillating walls, the energetic benefit obtained through the reduction of the friction drag has been computed and compared to the energetic cost of sustaining the lateral motion of the wall. It has been found that, when the oscillation velocity $v_{\theta 0}$ is small, the global energetic budget can be favourable: if the period T_w^+ lies between 100 and 150, a net power saving of up to 5–7% can be obtained. For values of the wall velocity higher than $v_{\theta 0}^+ \sim 7$, the power used for the movement of the wall is higher than the savings, and the global budget becomes negative.

4. Turbulence statistics

Detailed results are presented from the most resolved computation of the turbulent flow in a fixed pipe, in a steadily rotating pipe, and in a pipe which oscillates around its axis, sinusoidally in time, with a period of $T_w^+ = 100$ and with a rotation number $N = 0.5$, corresponding to an amplitude $v_{\theta 0}^+ \sim 7.1$. The oscillation period is the optimum in terms of drag reduction, while the value of the rotation number both determines an evident effect on wall turbulence and allows the flow to remain fully turbulent.

Some global quantities, computed for the turbulent flow in fixed, rotating and oscillating pipes, are shown in tables 1 and 2. They are compared with results from both numerical simulations and experiments, at equal or similar Reynolds numbers (Re_{cl} is based on the centreline velocity, and Re_τ on the friction velocity).

The ratio U_{cl}/U_b between the centreline velocity and the bulk mean velocity at $N = 0$ assumes in the present computation a value of 1.31 for the fixed pipe flow. This is identical (see table 2) to the results obtained by OF with a DNS at the same Reynolds number, and by EUW; it is moreover very near to the experimental values reported by EUW and by Reich & Beer (1989), even though their experiments were performed at a slightly higher Reynolds number. As already noted by EUW, this value for U_{cl}/U_b is significantly higher than the corresponding value in the plane channel flow, determined as $U_{cl}/U_b = 1.16$ for example in the work by Kim *et al.* (1987), possibly due to the effects of the friction over the 'side' walls of the pipe, which are absent in the case of plane channel flow. In the rotating case, the centreline mean velocity increases strongly, as shown by OF (measuring $U_{cl}/U_b = 1.44$) and by Reich & Beer ($U_{cl}/U_b = 1.35$). This is confirmed by the present computations, where the value of 1.42 is reached. The oscillating case, on the other hand, yields for the ratio U_{cl}/U_b a value of 1.34, which is closer to that of the fixed pipe flow. As will be shown later, in the oscillating case the axial mean velocity profile still retains a clearly turbulent shape, with a well-defined logarithmic region, while in the presence of steady rotation, as shown by OF, the same profile approaches the Poiseuille profile with increasing N. The shape factor:

$$H = \frac{\delta^*}{\theta} = \frac{\displaystyle\int_0^R \left(1 - v_z/U_{cl}\right) \mathrm{d}r}{\displaystyle\int_0^R v_z/U_{cl} \left(1 - v_z/U_{cl}\right) \mathrm{d}r}$$

	Fixed	Rotating	Oscillating
U_{cl}/U_b	1.31	1.42	1.34
U_b/u_τ	14.24	15.33	16.60
U_{cl}/u_τ	18.63	21.82	22.18
c_f	0.00986	0.00851	0.00726
c_f/c_{fo}	1.000	0.863	0.736
Re_{cl}	6419	6974	6566
Re_τ	172	160	148
δ^*	0.145	0.188	0.151
θ	0.089	0.109	0.085
H	1.63	1.72	1.78
$\lvert\Omega_z'\rvert^+$	4.65	5.16	5.02

TABLE 1. Comparison of global properties for mean turbulent flow in pipes: results from the present computations.

	Present	Orlandi & Fatica	Eggels *et al.* (DNS)	Eggels *et al.* (PIV)	Reich & Beer
U_{cl}/U_b	1.31	1.31	1.31	1.30	1.27
U_b/u_τ	14.24	14.41	14.73	14.88	14.59
U_{cl}/u_τ	18.63	18.87	19.31	19.38	18.53
c_f	0.00986	0.00963	0.00922	0.00903	0.00939
Re_{cl}	6419	6400	6950	7100	6350
Re	4900	4900	5300	5450	5000
Re_τ	172	170	180	183	171
H	1.63	1.64	—	—	—
H_c	1.85	—	1.86	1.83	—

TABLE 2. Global properties for mean turbulent flow in fixed pipes: numerical simulations and experiments.

for the mean axial velocity profile in the fixed and steady rotating cases agrees with the results from the computations by OF and the experimental data by Murakami & Kikuyama (1980), collected at higher Reynolds number. In the oscillating case, H reaches the higher value of $H = 1.78$.

Agreement is found also with the experimental and numerical results reported by EUW, where the displacement thickness δ_c^* and the momentum thickness θ_c are defined in cylindrical coordinates, and the resulting shape factor is $H_c = \delta_c^*/\theta_c$.

The steady rotation induces a reduction in the friction coefficient $c_f = \tau_w/\frac{1}{2}\rho U_b^2$ of 13.7% when comparing with the case at $N = 0$: this is in partial agreement with the result of OF, reporting approximately a 16% decrease, but is very similar to the experimental measurements performed by Reich & Beer (1989). The alternating oscillation of the pipe is more effective in drag reduction, leading to a 26.4% reduction in wall friction for the case considered here.

The radial distribution of the time-averaged mean axial velocity is shown in figure 3 for the three cases considered here. The effect of the steady rotation is to change the profile towards a more parabolic shape. In the oscillating case, however, the profile retains all of the features of a turbulent profile. The data set computed for $N = 0.5$ in the pipe with steady rotation is in very good agreement with the results obtained by OF, even though in their calculations the pipe length, the mesh size and even the radial distribution of the non-uniformity of the grid points are different (here a smoother stretching is applied throughout the pipe).

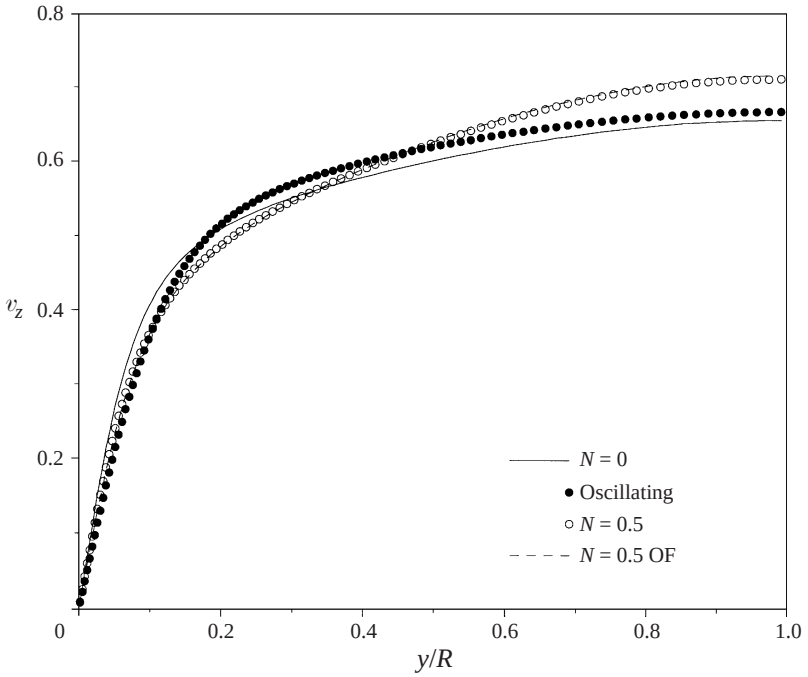

FIGURE 3. Mean streamwise velocity profiles, in outer variables, for fixed, steady rotating and oscillating pipe flows. Reference data from Orlandi & Fatica (1997) for the case of steady rotation.

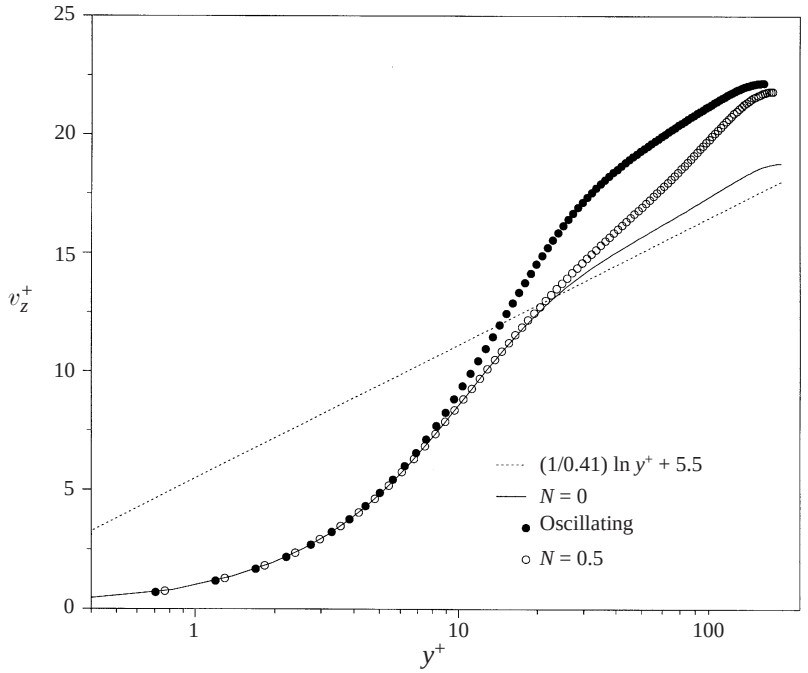

FIGURE 4. Mean streamwise velocity profile, in inner variables, for fixed, steady rotating and oscillating pipe flows.

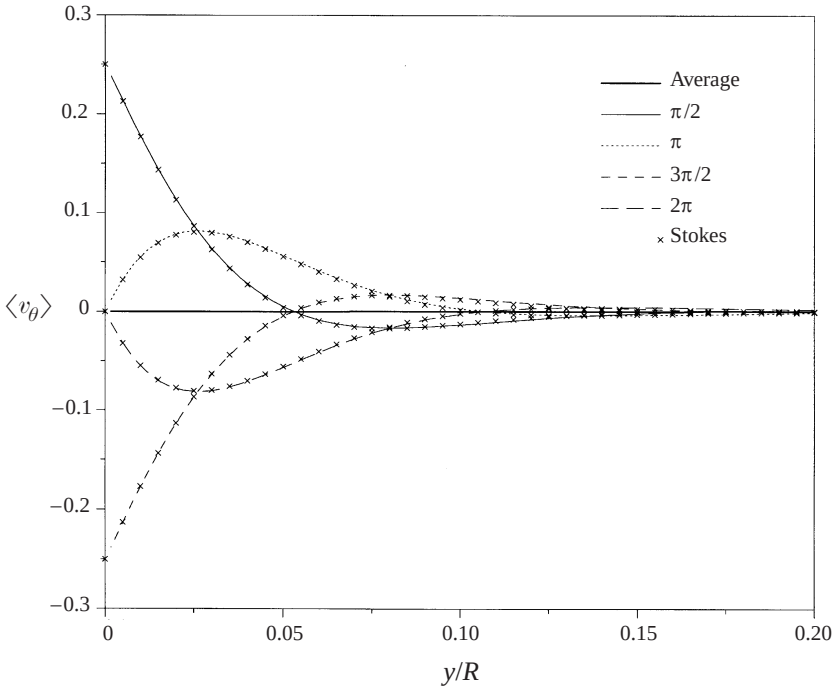

FIGURE 5. Phase-averaged radial profiles for the mean azimuthal velocity $\langle v_\theta \rangle$ (lines), compared with the Stokes' analytical laminar solution over a flat plate (symbols).

Examination of figure 4, where the same quantities are plotted in the usual law-of-the-wall form, allows the differences in the near-wall region to be seen more clearly. The profile for the fixed pipe flow shows that a departure from the usual channel law $u^+ = (1/0.41)\ln y^+ + 5.5$ is clearly established in the log and central regions, and confirms the high-resolution results of EUW and OF. The rotating pipe shows no evidence of a logarithmic region, while the oscillating case does present an upward-shifted linear region, with a slope parallel to the unmanipulated profile and which is typical of all the drag-reducing flows, as pointed out, among others, by Choi (1989). The amount of the upward shift, and the consequent increase in the viscous sublayer thickness, is comparable to that observed in plane channels with wall oscillation, as reported by Jung *et al.* (1992) and Baron & Quadrio (1996). This is not surprising, since it is known, as shown for example by Luchini (1996), that the upward shift is linearly related to the amount of drag reduction, which is comparable (see figure 2) for the two geometries.

When the pipe oscillates, the mean azimuthal velocity is zero. However averages taken at selected phases of the oscillation cycle are different from zero. This kind of average is indicated by $\langle\cdot\rangle$, while for the conventional time average the symbol $\overline{(\cdot)}$ is used. (In both cases, additional averaging over the homogeneous directions is applied.) The velocity components v_r and v_z are found not to show phase dependence; radial profiles of $\langle v_\theta \rangle$ are reported in figure 5 as a function of the phase of the oscillation.

This result agrees with the exact solution of the Stokes problem for an oscillating flat plate; this solution predicts for the Stokes layer a thickness $\delta^+ = \sqrt{4\pi T_w^+}$, which is ~ 35 in the present case. Computations and experiments, see e.g. Akhavana, Kamm & Shapiro (1991*a*, *b*), Sarpkaya (1993), Vittori & Verzicco (1998), show that transition

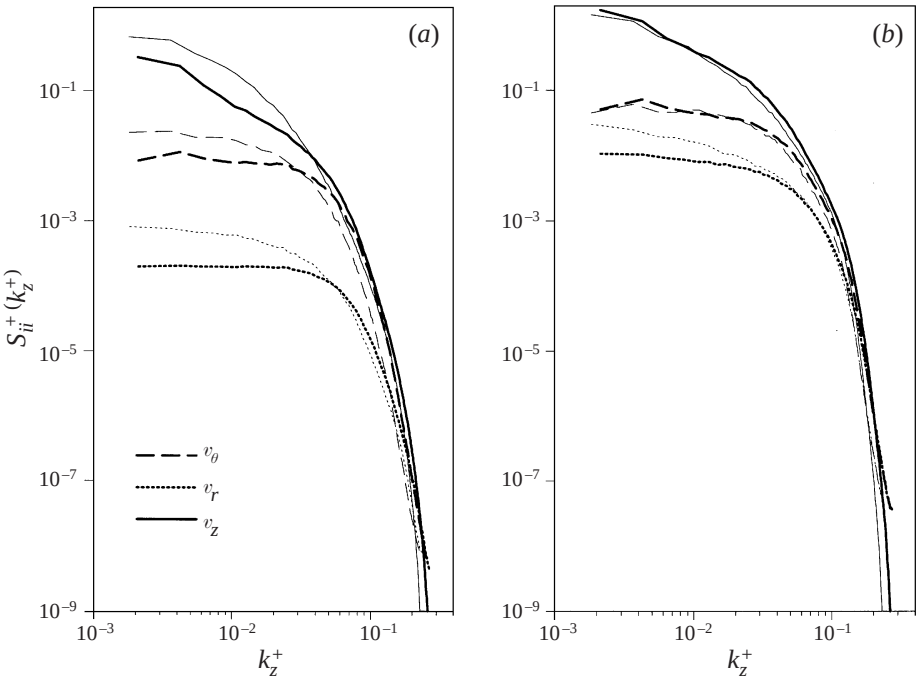

FIGURE 6. One-dimensional power spectral density functions, in the axial direction, for the velocity components (*a*) at $y^+ = 5$, and (*b*) at $y^+ = 20$. Thin lines refer to fixed pipe flow, and thick lines are for the oscillating pipe.

to turbulence in an oscillatory Stokes flow is observed at values of Re_δ, based on the thickness δ of the Stokes layer and the maximum transverse velocity of the wall, not less than 500, while Re_δ in the oscillating pipe flow under consideration here is 248. The simultaneous presence of laminar velocity profiles and finite levels of turbulent fluctuations in the accelerating phase has also been found in the simulation of Stokes flow transition performed by Akhavan *et al.* (1991*b*). The low value of the ratio between the thickness of the Stokes layer and the radius of the pipe implies small curvature effects, and explains the agreement between the Stokes laminar solution for the flat plate and the present results for a fully turbulent pipe flow.

The one-dimensional power spectral density functions for the velocity fluctuations in the axial direction, made non-dimensional in wall units, have been computed at different distances from the pipe wall. The spectra computed at $y^+ = 5$ and $y^+ = 20$ in the oscillating pipe flow, compared with the same quantities in the reference flow, are shown in figure 6(*a*, *b*). The first radial position has been chosen inside the transversal boundary layer generated by the spanwise oscillations, and the second one is in the buffer layer, where turbulent fluctuations are most significant. The spectra for the fixed pipe are consistent with those computed and measured by EUW. For the oscillating pipe, figure 6(*a*) shows near the wall a clear decrease in the energy content for all of the velocity components at low wavenumbers, i.e. for $k_z^+ < 0.04$. (Note that, as detailed in the following, for each computational case, the particular value of the friction velocity has been used; therefore this non-dimensionalization de-emphasizes the differences between the two datasets.) For $k_z^+ > 0.04$ the energy content for all the velocity components appears to be slightly increased. When the outer position is considered (figure 6*b*), the energy content for the longitudinal spectra is similar to

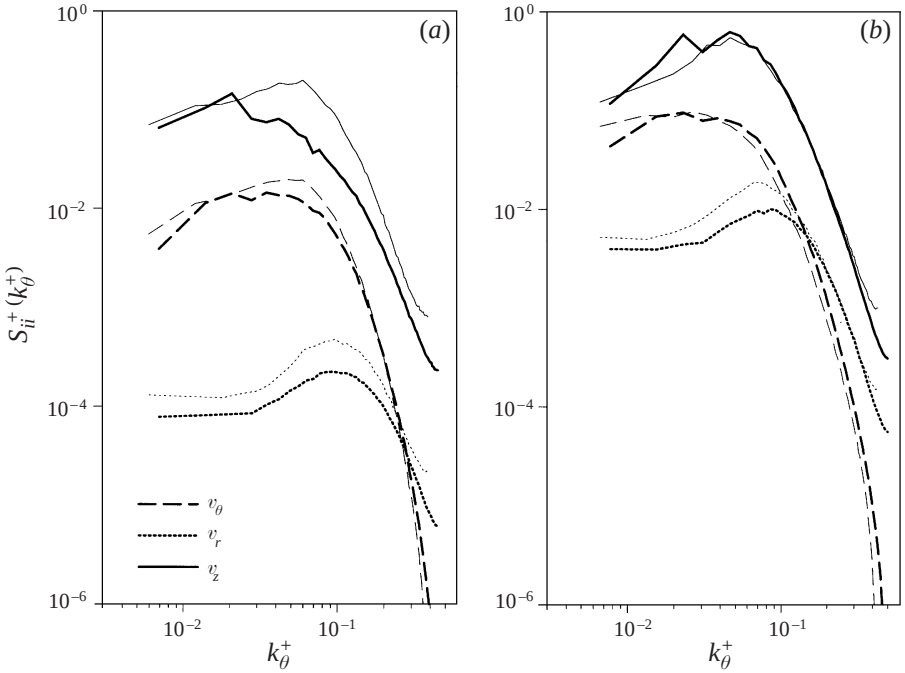

FIGURE 7. One-dimensional power spectral density functions, in the azimuthal direction, for the velocity components (*a*) at $y^+ = 5$, and (*b*) at $y^+ = 20$. Thin lines refer to fixed pipe flow, and thick lines are for the oscillating pipe.

that of the flow at $N = 0$ for the whole wavenumber range, with the exception of the radial component, which is reduced for a significant range of wavenumbers, even at $y^+ = 20$. Considered together, figures 6(*a*) and 6(*b*) indicate that at the highest longitudinal wavenumbers the energy content is low and without significant pile-up, thus suggesting that the axial resolution used in the present computations is adequate to resolve all the significant turbulent motions in the flow. The decay of the energy content of the axial component at the highest wavenumbers seems however to be marginally affected by numerical viscosity effects.

When the power spectral density functions in the azimuthal direction are considered, at the same positions (see figure 7*a*, *b*), it turns out that, at $y^+ = 5$, the very low-wavenumber spectrum for the streamwise component is essentially unchanged compared with that of the non-rotating pipe, while a reduction of the energy content is evident for higher wavenumbers. The azimuthal component is unchanged in the high-wavenumber range, and slightly reduced for lower wavenumbers. The spectrum for the radial velocity fluctuations is uniformly reduced over the full wavenumber range. This behaviour is consistent with the persistence of near-wall structures with average separation of the order of 100 wall units in the azimuthal direction. At the outer position, the differences with the reference case become less evident; one can however identify a slight reduction in the energy content for the lower half of the spectrum of the radial component. The observation made before on the adequacy of the axial resolution applies here also for the azimuthal direction.

Profiles, in the radial direction, of root-mean-square values for the velocity fluctuations are shown in figure 8(*a–c*) and compared with analogous quantities computed for the rotating and steady pipes. They are made non-dimensional by using for each

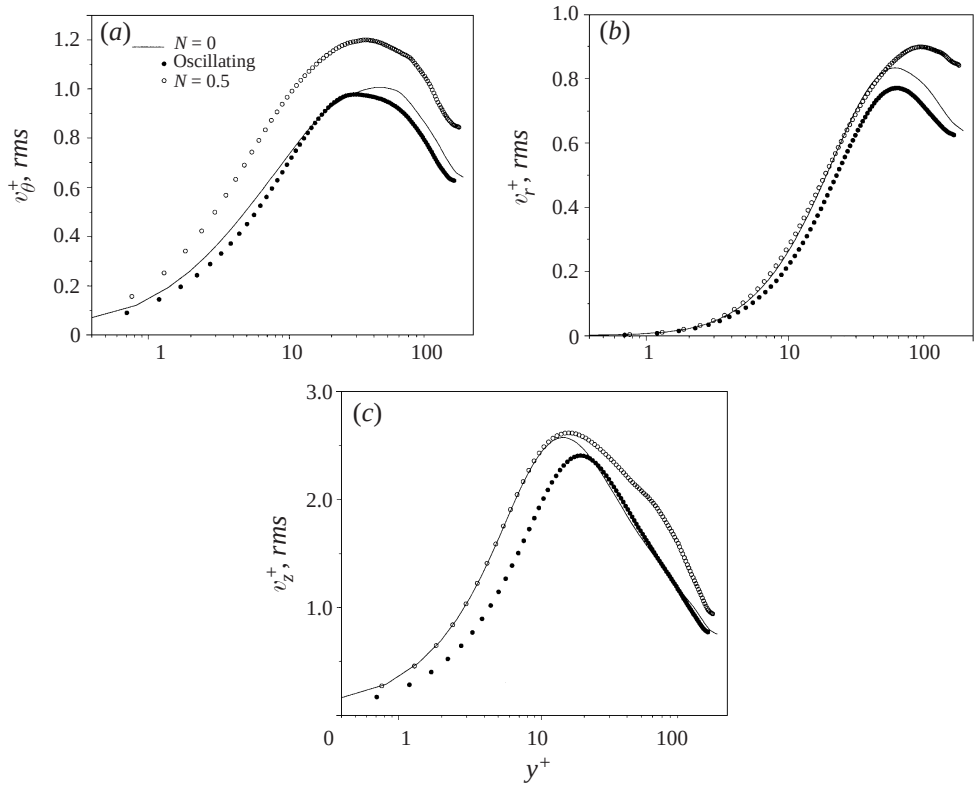

FIGURE 8. Radial profiles of root-mean-square velocity fluctuations, expressed in wall units: (*a*) v_θ; (*b*) v_r; (*c*) v_z.

case the value of the friction velocity u_τ computed in the simulation. For the fixed and steady rotating pipe flows, they agree with data from EUW and OF. When the pipe oscillates, the r.m.s. value of the tangential component is slightly reduced throughout the whole pipe, and shows a maximum closer to the pipe wall than the corresponding position in the reference case. Considerably higher values for the r.m.s. of v_θ are computed, as already pointed out by OF, when the pipe is subject to steady rotation. A reduction in the intensity of the fluctuations of the radial velocity component (figure 8*b*) is evident through the whole pipe; this reduction is not present in the rotating case. The axial component (figure 8*c*), on the other hand, presents a profile shifted at higher y for $y^+ < 20$, while its intensity is only slightly reduced and approaches the behaviour of the reference case in the outer part. This effect was not clearly reported in the simulations of turbulent channel flow subject to spanwise wall oscillations performed by Jung *et al.* (1992): in that study, all the values were made non-dimensional using a reference value for u_τ, corresponding to the friction in the unperturbed channel. Baron & Quadrio (1996), on the other hand, plot their results, computed for the plane channel at $Re_\tau = 200$, by using both reference and actual u_τ for non-dimensionalizing: when the actual u_τ is used, they compute approximately the same shift in the r.m.s. of the v_z profile as has been found in the present simulation for the oscillating pipe.

Phase-dependent radial distributions of root-mean-square velocity fluctuations have been computed, but they are not presented here, since no significant modifications in the profiles can be observed at different phases in the oscillation cycle.

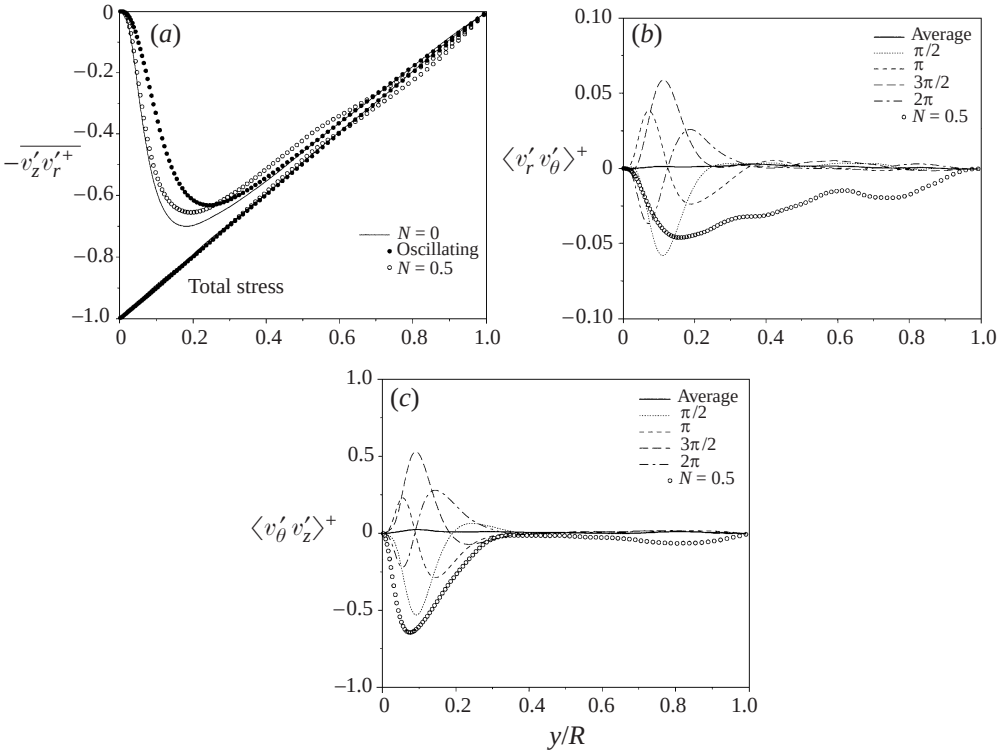

FIGURE 9. Mean and phase-averaged values of the Reynolds stress components, in wall units: (*a*) $-\overline{v_z' v_r'}^+$; (*b*) $\langle v_r v_\theta' \rangle^+$; (*c*) $\langle v_\theta' v_z' \rangle^+$.

The radial profile for the $-\overline{v_z' v_r'}$ component of the Reynolds stresses tensor is shown in figure 9(*a*). This component appears to be significantly reduced by the oscillation of the wall in the plane geometry, as noted by Jung *et al.* (1992) for the channel flow and by Laadhari *et al.* (1994) for the boundary layer. A similar reduction is found even in the case of the oscillating pipe. A reduction is also evident for the pipe in steady rotation, as observed by OF; the maximum of the profile is more or less the same, but the thickness of the near-wall region where the reduction takes place is lower for steady rotation. The total stress, i.e. the sum of the turbulent and viscous stresses, shows a linear profile for the steady and oscillating cases. This is an indication that the integration time has been chosen long enough for the flow to reach a statistically steady state. When the pipe is subjected to the steady rotation, however, the profile shows a slight departure from the linear behaviour. This has also been noted by OF, who relate the phenomenon to the presence of highly elongated structures in the central region of the pipe. Such elongated structures, observed both in experimental and numerical visualizations, induce modifications of the Reynolds stresses which greatly increase the time interval needed for complete convergence of the statistics to steady state, especially in the axial region of the pipe.

The other two extra-diagonal components of the Reynolds stress tensor are identically zero in the fixed pipe flow. This has to be the case, in a time-averaged sense, even in the oscillating pipe flow, but non-zero profiles do appear when the phase averages are considered. The steady rotating pipe exhibits non-zero profiles even for time-mean values. The radial profile of $\langle v_r' v_\theta' \rangle$ (see figure 9*b*) shows, for steady rotation, a distribution similar to that of the $-\overline{v_z' v_r'}$ component, but with a magnitude approximately

one order lower. A phase dependence is found for $\langle v_r' v_\theta' \rangle$, with symmetry in the two halves of the cycle. The time-averaged value is close to zero, and the non-zero values at each phase extend far from the wall. The profiles for phase angles corresponding to the maximum wall velocity are comparable in intensity with the distribution of the same component in the steady rotating case. Even the $\langle v_\theta' v_z' \rangle$ component, plotted in figure 9(*c*), shows this phase dependence, with a similar symmetry and a zero time average. The peak values near the wall have the same order of magnitude as those of $-\overline{v_z' v_r'}$. The maxima at a phase angle of $\pi/2$ and $3/2\pi$ occur at $y/R = 0.1$ and reach values very close to those computed in the steady rotating case. At π and 2π a second peak value of opposite sign is found at $y/R = 0.06$, and another zero-crossing occurs at $y/R = 0.10$.

The analysis of the Reynolds stress profiles confirms the suggestion, made by Dhanak & Si (1999), that the transport of momentum in the direction normal to the wall is reduced, as indicated by the decrease of the $\overline{v_z' v_r'}$ Reynolds stress level. Furthermore, the radial profile for $\langle v_r' v_\theta' \rangle$ shows a negative peak at a phase angle of $\pi/2$, i.e. in the first quarter of the oscillation cycle, when at the wall the transverse velocity $v_\theta = +v_{\theta 0}$ is maximum; this means that fluid which travels away from the wall is predominantly associated with positive v_θ', and vice versa (remember that v_r is positive when directed towards the pipe wall). In the opposite phase of the oscillation, at $3\pi/2$, the situation is reversed, due to the change of sign of v_θ. Since $\overline{v_z' v_r'}$ is positive, the fluctuations v_z' and v_r' tend to have the same sign, and $\langle v_\theta' v_z' \rangle$ should hence have the same sign as $\langle v_r' v_\theta' \rangle$, as confirmed by figure 9(*c*). This analysis suggests that, when the wall speed is maximum, ejection events are mostly associated with positive values of the fluctuations of $|v_\theta|$ around its phase-averaged mean value. Conversely, sweep-type events are mostly associated with negative fluctuations of $|v_\theta|$.

In figure 10 the quadrant decomposition of the $-\overline{v_z' v_r'}$ Reynolds stress component is reported. The sign of the radial component has been changed, in order to allow the customary terminology which refers to ejections as events pertaining to the second quadrant, and sweeps to the fourth. In the case of $N = 0$, one can note the general agreement with the results of Kim *et al.* (1987) for the plane channel flow. When considering time-averaged data for the oscillating pipe over the full cycle, Q1- and Q4-type events, which are connected with high longitudinal velocity and are the dominant contributors in the near-wall region, both increase significantly their percentage contribution with respect to the reference flow. In particular the contribution of Q1 events is more than doubled. When phase dependence is taken into account, some effects are visible only in the near-wall region.

Further statistical moments (skewness and flatness factors) for the fluctuations of the velocity components are shown in figure 11(*a*, *b*). Both agree well with the data reported by EUW, concerning the statistics of steady pipe flow, confirming the different behaviour of the flatness factor for v_r in plane and cylindrical geometry, related by EUW to an altered 'splatting' effect due to transverse curvature. The third moment of the tangential velocity component, being zero for symmetry, is practically unaffected by the oscillation, and further indicates the adequacy of the statistical sample used for the averages. The skewness factor for the other two velocity components shows an increase in the inner part of the pipe. The skewness of v_z at the wall is almost doubled, indicating a higher probability for large positive fluctuations of v_z than for large negative ones. The flatness factor, on the other hand, is significantly increased for all three components in the near-wall region, indicating an overall tendency to a more intermittent behaviour.

Two-point velocity correlations are illustrated in the following, computed both for

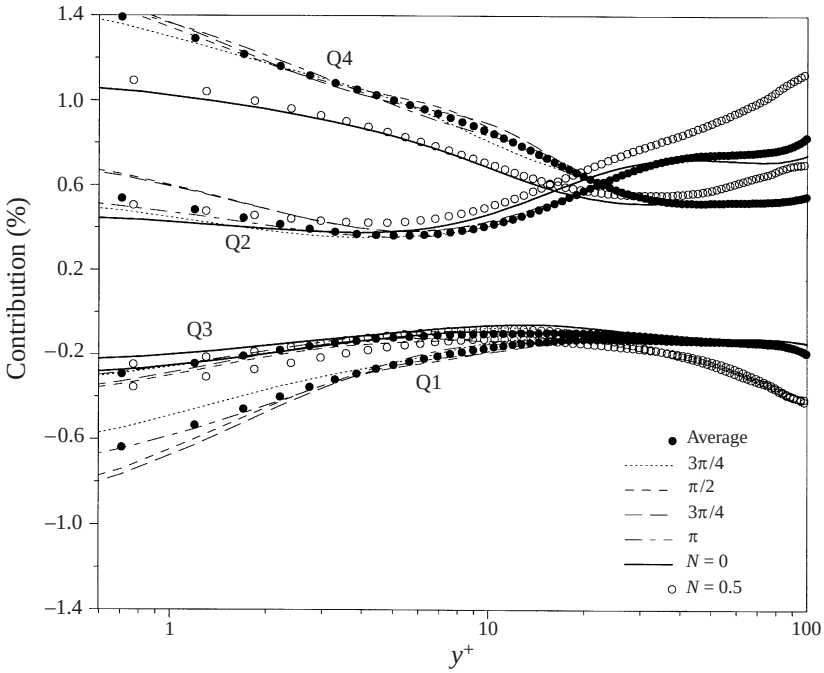

FIGURE 10. Mean and phase-averaged quadrant analysis for the component $-\overline{v_z' v_r'}$ of the Reynolds stress tensor.

the longitudinal and azimuthal directions. Both the time-averaged and phase-averaged versions are presented. The correlation coefficient $R_{\theta\theta}(z)$ for the v_θ component in the streamwise direction, computed for the near-wall position at $y^+ = 5$, is shown in figure 12(*a*). Remember that the actual length of the pipe is $L = 20R$: here only the first part of the correlation function is shown. Comparing with the case at $N = 0$, the correlation decreases faster, with some dependence on the phase, while in the steady rotating pipe the decrease is slower, going to zero in approximately 3 times the downstream distance. A similar behaviour is observed for $R_{rr}(z)$ (figure 12*b*). For the streamwise component of the velocity, the coefficient $R_{zz}(z)$ in figure 12(*c*) shows, as already pointed out in § 2, that a pipe length of $L = 20R$ is sufficient for the numerical simulation of this flow using periodic boundary conditions in the axial direction. A significant increase in the streamwise scale of the correlation, due to the drag-reducing action of the oscillations, is evident: this is a substantial difference with the case of steady rotation, where this coefficient does not undergo any appreciable modification.

The axial correlations computed at $y^+ = 20$ (not shown) make it clear that, at this distance from the wall, all of the modifications induced in the streamwise correlation functions by the oscillation of the pipe have disappeared, except for the increment of the streamwise length scale, which is still evident even at $y^+ = 100$.

Concerning the correlation functions in the azimuthal direction at $y^+ = 5$, while their phase dependence is not remarkable (and consequently not reported here), their time-averaged behaviour (figure 13*a–c*) is significantly affected by the alternating oscillation of the pipe wall, except for the coefficient for the radial component, $R_{rr}(\lambda^+)$, which is quite similar to the reference case. The well-known minimum at a spanwise separation of approximately 50 wall units, present in the reference case

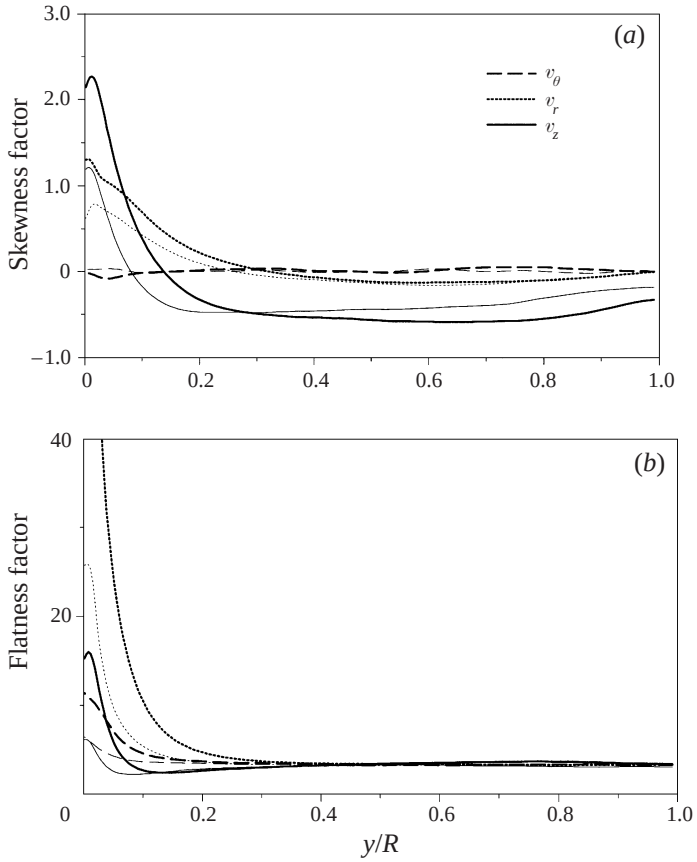

FIGURE 11. (*a*) Skewness, and (*b*) flatness factors for the three velocity components: thin lines refer to the fixed pipe, and thick lines to the oscillating pipe.

for $R_{\theta\theta}(\lambda^+)$ and $R_{zz}(\lambda^+)$, is reduced by the oscillations for the azimuthal component, and almost disappears for the longitudinal component. This is a further indication that a strong modification of the near-wall turbulence structures takes place as a consequence of the alternating oscillation of the pipe wall. Examining the same quantities far from the wall (plots not shown here), one sees that the effects of the alternating oscillation fade away as the centre of the pipe is approached. Near the pipe centreline, the coefficients do not fall to zero, since, as put forward by Eggels *et al.* (1994), in this region the velocity fluctuations are strongly correlated in the azimuthal direction, due to small separation distances.

These relevant effects of the oscillations on the correlation functions can be explained by the convective action of the Stokes layer on the near-wall part of the turbulent structures. The lateral shift induced by the layer can be estimated from the Stokes solution, by integrating in time the velocity law from zero to the first half of the period. This gives a transversal displacement of approximately 180 wall units at $y^+ = 5$, and 80 at $y^+ = 10$. The turbulent structures in the lower buffer layer hence are displaced by about 100 wall units, while above the Stokes layer they remain relatively undisturbed; this is confirmed by the spanwise correlation coefficient of v_z' at $y^+ = 20$ (not shown), which still presents the usual minimum point at $\lambda^+ \simeq 50$, while at $y^+ = 5$ (figure 13*c*) the minimum has completely disappeared.

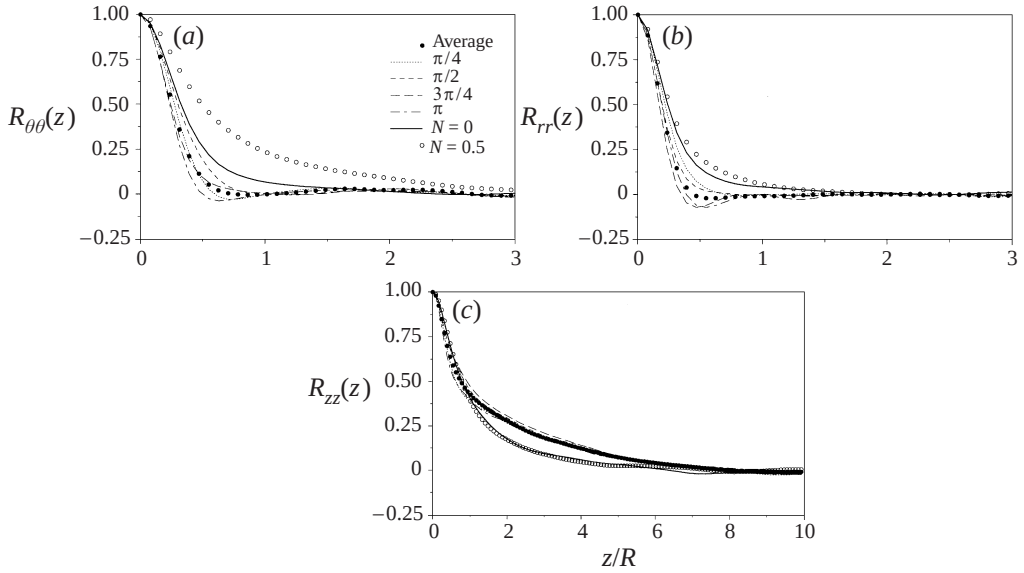

FIGURE 12. Axial correlations of velocity fluctuations at $y^+ = 5$: (*a*) v_θ; (*b*) v_r; (*c*) v_z. Note the different axis scale for (*c*).

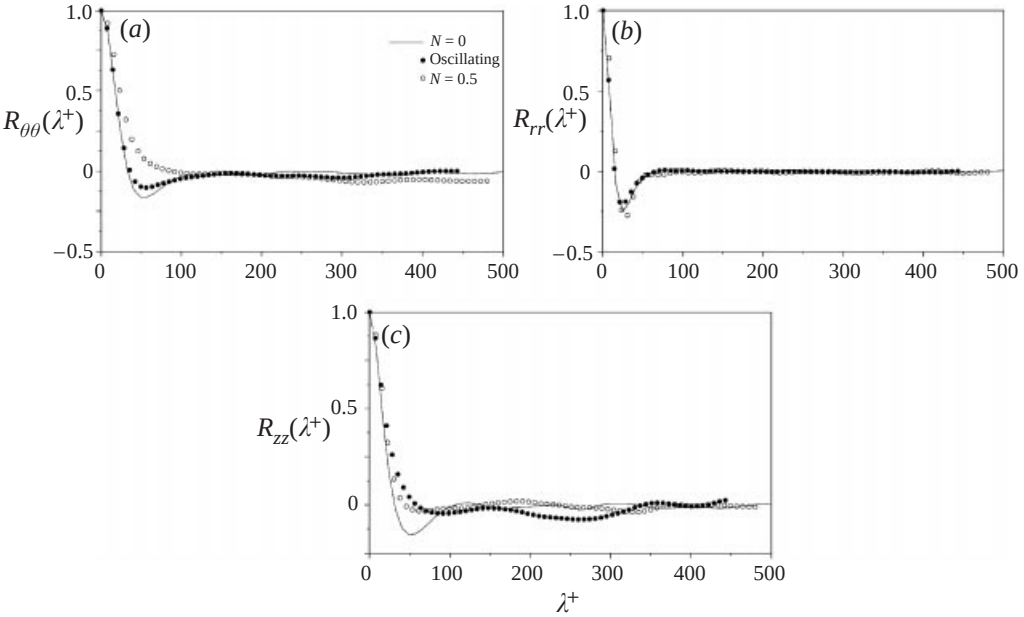

FIGURE 13. Azimuthal correlations of velocity fluctuations at $y^+ = 5$: (*a*) v_θ; (*b*) v_r; (*c*) v_z.

The near-wall distortion of the streaky pattern determines the presence, at certain phases of the cycle, of regions of high axial velocity stacked over regions of low axial velocity near the wall, and vice versa. This implies high radial gradients of streamwise velocity fluctuations, and hence high values of ω'_θ, at $y^+ \simeq 10$. Indeed, the analysis of the phase-averaged root-mean-square ω'_θ radial profiles (figure 14*a*) shows a maximum which appears in the acceleration phase of the cycle (at $\pi/4$) at

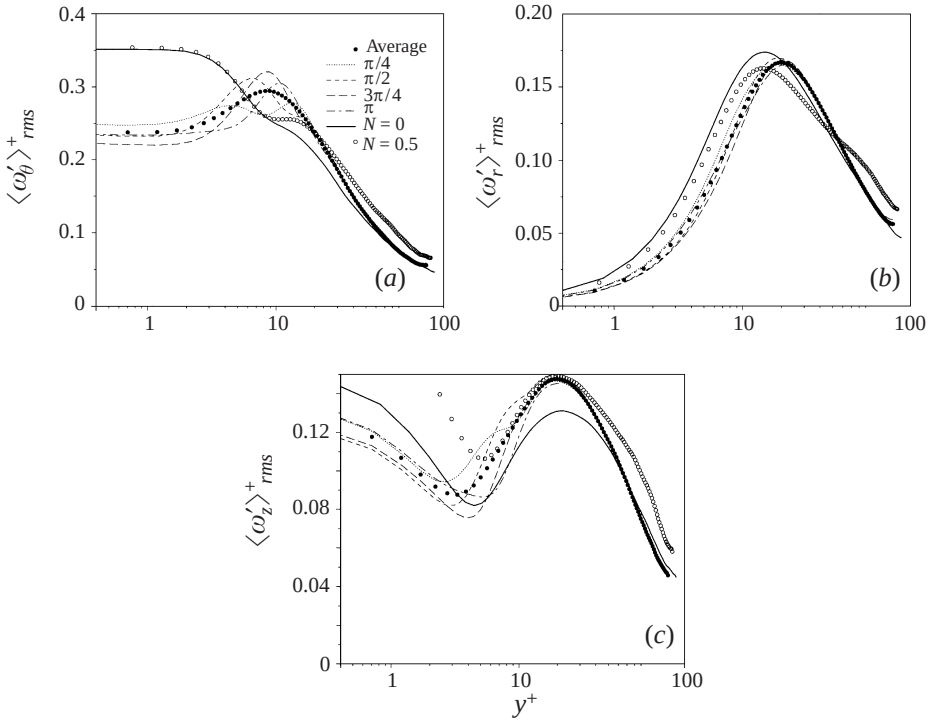

FIGURE 14. Radial profiles of phase-averaged root-mean-square vorticity fluctuations, expressed in wall units, for: (*a*) ω'_θ; (*b*) ω'_r; (*c*) ω'_z.

$y^+ = 4$, grows during the rest of the cycle reaching $y^+ = 11$ at π and fades away at the beginning of the counter-rotating phase (the curve at $5/4\pi$ is coincident with the one at $\pi/4$).

The tangential displacement of near-wall fluid, and the consequent stretching of the structures, can also be visually appreciated by looking at figure 15(*a*, *b*), where a contour plot in a cross-section field for ω'_r is plotted, comparing the fixed and the oscillating pipe. The alternating movement of the wall appears to limit the vertical development and coherence of the structures, and to amplify their lateral dimensions. The most evident difference between figures 15(*a*) and 15(*b*) is in the vertical displacement of the structures in the oscillating pipe: their near-wall part is stretched, while the outer part is less sensitive to the Stokes layer.

A clear alternating structure of low-speed and high-speed streaks is therefore maintained only above the upper limit of the Stokes layer. This explains why the ω'_r radial profile (figure 14*b*) exhibits an outward shift of about 10 wall units, which is a distance of the order of the layer thickness, and why the same profile turns out to be almost phase-independent.

Figure 16(*a–c*) shows how the oscillations of the pipe modify the velocity streaks inside the Stokes layer. In the reference case (figure 16*a*), there are clearly elongated streaks of low-speed fluid with interposed high-speed, less elongated areas. The same qualitative picture emerges (figure 16*b*) for the pipe in steady rotation, where one can however observe, as reported by OF, a greater spacing between the streaks, and a tilting of the structures. The picture is different when the pipe oscillates; the intensity of the streaky structures is reduced, and although some high-speed spots are present,

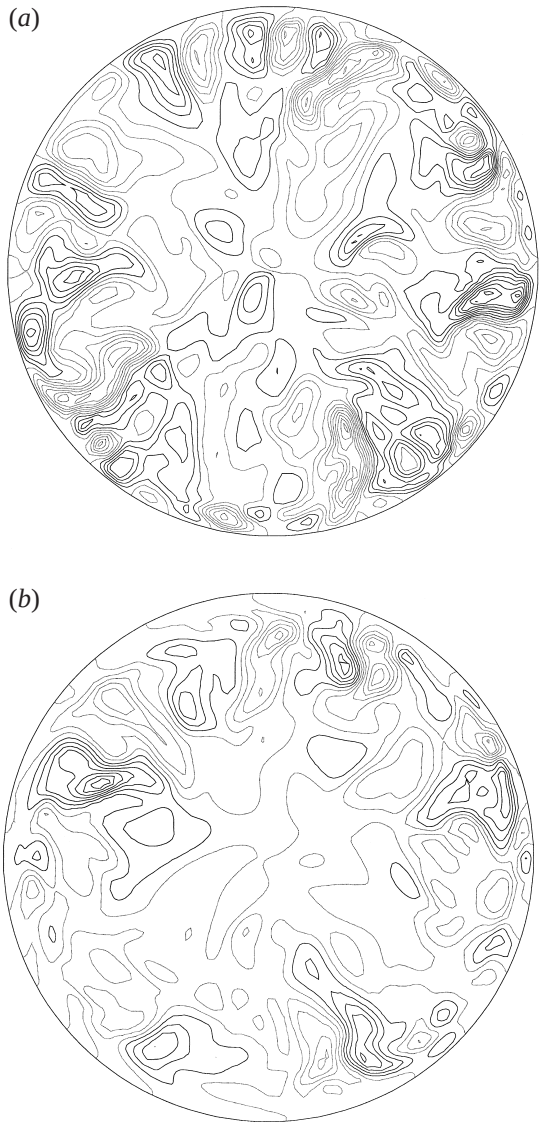

FIGURE 15. Contour plot of ω_r, in a cross-section of (*a*) the steady pipe, and (*b*) the oscillating pipe. Darker lines indicate positive values, increment is 0.2.

the evidence of elongated low-speed streaks is totally lost; this scenario is consistent with the increase of the flatness factor in the near-wall region.

Quasi-streamwise vortical structures are less affected by wall oscillation. Speculative arguments put forward by Kim *et al.* (1987) and considerations drawn from coherent structure eduction, performed by Jeong *et al.* (1997) for a plane channel, indicate that the average position of streamwise vortical structures lies between 10 and 30 wall units from the wall, i.e. mostly outside the Stokes layer created by the wall oscillation. The time-averaged radial profile of root-mean-squared ω_z' (figure 14*c*) has a maximum at $y^+ \simeq 20$, which is similar to the reference case and further suggests that the average position of streamwise vortices could be unmodified. The second maximum which appears in the various phase-averaged profiles and moves toward

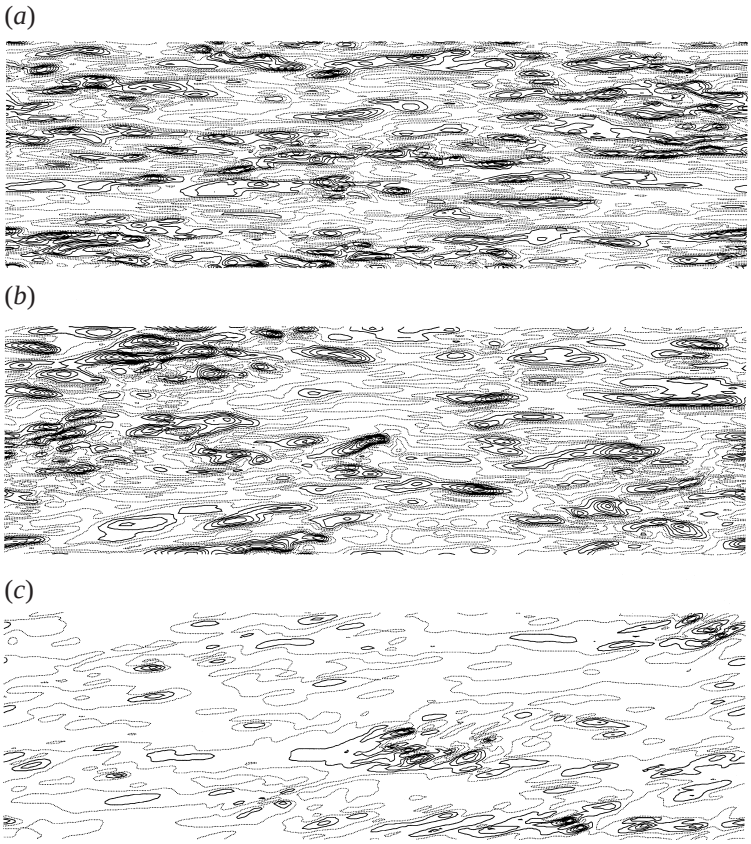

FIGURE 16. Instantaneous flow field of v_z at $y^+ = 5$: (*a*) fixed pipe; (*b*) steady rotating pipe; (*c*) oscillating pipe. Darker lines indicate positive values, increment is 0.015.

the centre of the pipe during the acceleration phase can be interpreted as a trace of a layer of secondary streamwise vorticity, generated by the oscillation, which moves upwards, with a mechanism similar to that proposed above to explain phase-averaged profiles of ω'_θ.

In any case, the presence of this secondary, superimposed pattern does not allow determination of, purely from an examination of the radial profile of the r.m.s. value of the ω_z fluctuations, whether the intensity of streamwise vortices is reduced or not in the oscillating pipe flow. A tentative approach in this direction has been made by Miyake, Tsujimoto & Takahashi (1997), who analysed the turbulent flow in a plane channel of half-width h, where only one wall oscillates. They studied the evolution in time of a quantity called total streamwise vorticity, defined as

$$|\Omega'_z|^+ = \frac{\nu}{h u_\tau} \int_{\mathscr{V}} |\omega'_z| \, \mathrm{d}\mathscr{V},$$

where u_τ is the mean friction velocity. $|\Omega'_z|^+$ is computed by integrating the absolute value of streamwise vorticity fluctuations over each half $\mathscr{V}$ of the computational domain, and by translating the dimensional result in plus units with the value of the friction velocity averaged over the two sides of the channel. They found that on the oscillating side $|\Omega'_z|$ assumes values lower than on the steady side, and therefore concluded that an effect of the oscillation of the wall is to reduce the intensity of

quasi-streamwise vortices. In their paper, this is then related to a reduction of the vortex stretching, leading to less conversion of spanwise vorticity into streamwise vorticity, and thus to a partial suppression of the key process of self-sustenance for the streamwise vortices.

It should be noted, however, that the values of $|\Omega_z'|$ in the two sides would be much closer if the non-dimensionalization were made with the friction velocities particular to each side. The present computations, for example, yield a slightly increased value for the total streamwise vorticity in the oscillating pipe flow (see table 1), when using the friction velocity computed for the same flow: a value of 5.02, compared to 4.65 for the reference flow.

The persistence of quasi-streamwise vortical structures only outside of the Stokes layer is responsible for the presence of streaky velocity patterns in the near-wall region, which can be inferred from the autocorrelation functions for the velocity components, shown in figures 12 and 13. The disappearance of the minimum point for $R_{zz}(\lambda^+)$ can be explained by reasoning that fluid with low axial velocity (hence with predominantly negative v_r, due to the sign of $\overline{v_z' v_r'}$) is convected by the Stokes layer into a region where $v_r > 0$ and $v_z < 0$, due to the pumping action of the outer vortex. The low-speed fluid therefore remains near the wall, and the v_z fluctuations are thereby reduced. The opposite process leads to the same effect when fluid with high axial velocity is considered. This effect is responsible for the appearance of additional counter-gradient Reynolds stresses, as seen by the increased relative role of Q1 and Q3 events in the oscillating pipe flow (figure 10). For the v_r and v_θ components, a streaky pattern should persist, since it is induced mainly by the external action of the quasi-streamwise vortices, which are relatively unaffected outside the Stokes layer.

5. Discussion

A comparison of the turbulent flow with and without an alternating movement of the pipe wall indicates that the skin friction drag reduction induced by the oscillations can be due to the tangential advection by the Stokes layer. The effects are more evident on the flow structures in the viscous sublayer and in the near-wall buffer layer, while the average position of the outer, quasi-streamwise vortical structures is less affected, when the frequency of the oscillation (and consequently the thickness of the Stokes layer) are set to values which lead to significant drag reduction.

A simplified description of the interaction between the movement of the wall and the turbulence structures has been recently reported by Dhanak & Si (1999), who used an extension of the two-dimensional flow model developed by Orlandi & Jiménez (1994) for studying the effects of wall oscillation upon a pair of counter-rotating streamwise vortices, and included the additional effect of vortex stretching.

The two-dimensional assumption of Orlandi & Jiménez (1994) can be considered a good approximation for phenomena, in the (r, θ)-plane, whose characteristic time scale is significantly smaller than the time scale associated with the longitudinal variations of the flow. In the present case, two-dimensional computations can be thought of as representative of the real three-dimensional events for approximately 20 viscous time units, as estimated by Orlandi & Jiménez (1994), while the time scale of a single oscillation of the wall is $O(100)$ viscous time units. Moreover, $O(10)$ such oscillations are found to be needed before the pressure gradient adjusts to its new mean value and the flow becomes statistically steady. This simple comparison of time scales makes it clear that the oscillation of the wall not only has an immediate effect on the existing flow structures, but it also affects their regeneration cycle in a significant way.

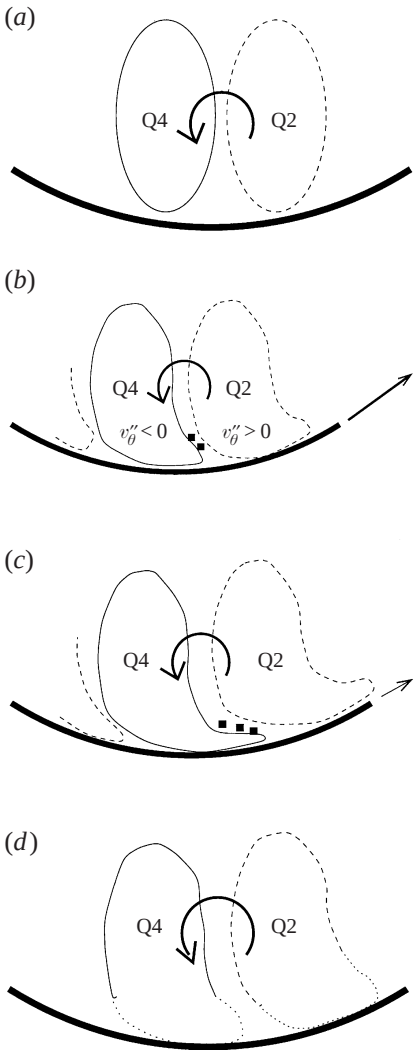

FIGURE 17. Conceptual model of the coherent structure dynamics during one half of the oscillation cycle. Phase angles of: (*a*) 0; (*b*) $\pi/2$; (*c*) $3\pi/4$; (*d*) π.

In addition, the initial distance from the wall at which the vortex pair is placed appears to be a crucial parameter. If the pair, as in Dhanak & Si (1999), is located at a distance of $y^+ \sim 10$ from the wall, the vortices are partially embedded in the Stokes layer, and can go through direct distortion by the movement of the wall. On the basis of the turbulence statistics presented in § 4, see in particular figure 14(*c*), it is possible to think of the quasi-streamwise vortices as staying in an outer position, typical of the reference flow, relatively unaffected by the motion of the wall and remaining mainly outside the Stokes layer. According to this idea, the interaction between a single quasi-streamwise vortex and the moving wall can be qualitatively described as follows.

At the beginning of the accelerating phase, the turbulent structures in the buffer layer are supposed to show a pattern similar to that of the reference flow, as described, for instance, by Jeong *et al.* (1997) in the analysis of plane channel flows. A single

quasi-streamwise vortex, indicated by the arrow in figure 17(*a*), is assumed to have streamwise component of vorticity of the same sign as the vorticity induced by the movement of the wall. The vortex, with axis located at the average position of $y^+ = 20$, advects low-streamwise-velocity fluid outwards from the wall (Q2 event, region of fluid enclosed by the dashed line in the figure) and high-streamwise-velocity fluid towards the wall (Q4 event, region of fluid enclosed by the continuous line).

At a phase angle of $\pi/2$ the velocity of the wall reaches its maximum value. The resulting Stokes layer causes a skewing of near-wall (i.e. $y^+ < 10$) low- and high-speed regions in the direction of the mean tangential flow, as shown in figure 17(*b*). Consequently, a stacking of low- and high-speed regions takes place: high-speed fluid near the wall happens to be located below a region of low-speed fluid in the buffer layer, and vice versa. This stacking generates, at $y^+ \simeq 10$, regions of high shear $\partial v_z'/\partial r$, already noted in discussing figure 14(*a*), and indicated in figure 17(*b*) by the black squares. Moreover, as reported in the context of figure 9(*c*), the induction by the quasi-streamwise vortex leads to advection of high-tangential-velocity fluid from the wall region (within the low-speed streak) and of low-tangential-velocity fluid towards the wall region (within the high-speed streak).

During the decelerating phase (figure 17*c*), the skewing and stacking of streaky structures is enhanced: the advection induced by the quasi-streamwise vortex, whose position is less affected by the Stokes layer, contributes in moving high-speed fluid far from the wall, thus generating counter-gradient Reynolds stresses (Q1 events, figure 10).

Owing to the effect of these shear layers, the local radial gradients of axial velocity in the Stokes layer are smoothed. At a phase angle of π, the intensity of axial velocity fluctuations is therefore reduced in both low- and high-speed regions (dotted contour lines in figure 17*d* for the v_z component): this effect has been reported in figure 8(*c*).

This crude description, which neglects all the three-dimensional effects which are present in the real flow, is nevertheless able to establish some links between the evolution of the near-wall structures and the modifications to the turbulence statistics illustrated in § 4.

6. Conclusions

We have studied, via direct numerical solution of the Navier–Stokes equations, the drag-reducing turbulent flow in a pipe oscillating around its longitudinal axis, by comparing it to the reference turbulent flow in a fixed pipe and in a pipe with steady rotation.

Numerical experiments have quantified the maximum amount of friction drag reduction achievable with this technique as 40%. It is possible however that this maximum could be slightly lower at higher Reynolds numbers. When the velocity of the oscillating wall is low, the energetic benefits of drag reduction can be 5–7% greater than the costs of sustaining the oscillation of the pipe.

The main feature of the flow is the formation of a periodic near-wall transversal boundary layer, with azimuthal velocity profiles almost coincident with the analytical solution of the Stokes problem for the oscillating flat plate. A detailed analysis of the turbulence statistics, collected both by time-averaging and averaging over phases, has been presented, supporting the idea that the Stokes layer induces a skewing of the near-wall portion of the elongated low- and high-speed streaks, and results in a displacement with respect to the quasi-streamwise vortical structures in the buffer layer. This relative lateral displacement, which is particularly evident for low-speed

regions, is thus responsible for reducing the contribution of the ejection events to the Reynolds stresses in the flow, and eventually the skin-friction drag.

The authors are grateful to Paolo Orlandi and Roberto Verzicco for the use of their computer code, and the useful suggestions, discussions, encouragement and support. We acknowledge the support of CILEA (Consorzio Interuniversitario Lombardo per l'Elaborazione Automatica) for providing part of the necessary computational resources. This work was financially supported by MURST in 1995 and ASI in 1999. Part of the research has been presented at the 3rd ERCOFTAC Workshop on Vortex Dynamics in Rotating Systems, Aussois, France, 1997.

REFERENCES

Akhavan, R., Kamm, R. D. & Shapiro, A. H. 1991*a* An investigation of transition to turbulence in bounded oscillatory Stokes flows. Part 1. Experiments. *J. Fluid Mech.* **225**, 395–422.

Akhavan, R., Kamm, R. D. & Shapiro, A. H. 1991*b* An investigation of transition to turbulence in bounded oscillatory Stokes flows. Part 2. Numerical simulation. *J. Fluid Mech.* **225**, 423–444.

Baron, A. & Quadrio, M. 1996 Turbulent drag reduction by spanwise wall oscillations. *Appl. Sci. Res.* **55**, 311–326.

Choi, K.-S. 1989 Near-wall structure of a turbulent boundary layer with riblets. *J. Fluid Mech.* **208**, 417–459.

Choi, K.-S. & Graham, M. 1998 Drag reduction of turbulent pipe flows by circular-wall oscillation. *Phys. Fluids* **10**, 7–9.

Choi, K.-S., Roach, P., DeBisschop, J. R. & Clayton, B. 1997 Turbulent boundary-layer control by means of spanwise-wall oscillation. *AIAA Paper* 97-1795.

Dhanak, M. R. & Si, C. 1999 On reduction of turbulent wall friction through spanwise wall oscillations. *J. Fluid Mech.* **383**, 175–195.

Eggels, J. G. M., Unger, F., Weiss, M. H., Westerweel, J., Adrian, R. J., Friedrich, R. & Nieuwstadt, F. T. M. 1994 Fully developed turbulent pipe flow: a comparison between direct numerical simulation and experiment. *J. Fluid Mech.* **268**, 175–209 (referred to herein as EUW).

Kim, J., Moin, P. & Moser, R. 1987 Turbulence statistics in fully developed channel flow at low Reynolds number. *J. Fluid Mech.* **177**, 133–166.

Laadhari, F., Skandaji, L. & Morel, R. 1994 Turbulence reduction in a boundary layer by a local spanwise oscillating surface. *Phys. Fluids* A **6**, 3218–3220.

Luchini, P. 1996 Reducing the turbulent skin friction. In *Computational Methods in Applied Sciences 1996*. Proc. 3rd ECCOMAS CFD Conference (ed. J.-A. Desideri *et al.*), pp. 466–470. Wiley.

Jeong, J., Hussain, F., Schoppa, W. & Kim, J. 1997 Coherent structures near the wall in a turbulent channel flow. *J. Fluid Mech.* **332**, 185–214.

Jung, W. J., Mangiavacchi, N. & Akhavan, R. 1992 Suppression of turbulence in wall-bounded flows by high-frequency spanwise oscillations. *Phys. Fluids* A **4**, 1605–1607.

Miyake, Y., Tsujimoto, K. & Takahashi, M. 1997 On the mechanism of attenuation of turbulence by spanwise wall oscillation. In *Direct and Large-Eddy Simulation II* (ed. J. P. Chollet *et al.*), pp. 201–212. Kluwer.

Murakami, M. & Kikuyama, K. 1980 Turbulent flow in axially rotating pipes. *J. Fluids Engng Trans. ASME* I: **102**, 97–103.

Orlandi, P. & Fatica, M. 1997 Direct simulations of turbulent flow in a pipe rotating about its axis. *J. Fluid Mech.* **343**, 43–72 (referred to herein as OF).

Orlandi, P. & Jiménez, J. 1994 On the generation of turbulent wall friction. *Phys. Fluids* **6**, 634–641.

Reich, G. & Beer, H. 1989 Fluid flow and heat transfer in axially rotating pipe. 1. Effect of rotation on turbulent pipe flow. *Intl J. Heat Mass Transfer* **32**, 551–561.

Robinson, S. K. 1991 Coherent motions in the turbulent boundary layer. *Ann. Rev. Fluid Mech.* **23**, 601–639.

Sarpkaya, T. 1993 Coherent structures in oscillatory boundary layers. *J. Fluid Mech.* **253**, 105–140

Skandaji, L. 1997 Etude de la structure d'une couche limite turbulente soumise à des oscillations transversales de la paroi. PhD thesis, Ecole Centrale de Lyon, France.

Trujillo, S. M., Bogard, D. G. & Ball, K. S. 1997 Turbulent boundary layer drag reduction using an oscillating wall. *AIAA Paper* 97-1870.

Verzicco, R. & Orlandi, P. 1996 A finite difference scheme for direct simulation in cylindrical coordinates. *J. Comput. Phys.* **123**, 402–413.

Vittori, G. & Verzicco, R. 1998 Direct simulation of transition in an oscillatory boundary layer. *J. Fluid Mech.* **371**, 207–232.